Inorganic Chemistry

Article

pubs.acs.org/IC

Zinc Chalcogenolate Complexes as Precursors to ZnE and Mn/ZnE (E = S, Se) Clusters

Chhatra B. Khadka,[†] Andreas Eichhöfer,[‡] Florian Weigend,*[,‡] and John F. Corrigan*[,†,§]

[†]Department of Chemistry, The University of Western Ontario, London, Ontario, N6A 5B7 Canada

[‡]Institute of Nanotechnology, Karlsruhe Institute of Technology, Hermann-von-Helmholtz-Platz 1, 76344 Eggenstein-Leopoldshafen, Germany

[§]Centre for Advanced Materials and Biomaterials Research, The University of Western Ontario, London, Ontario, N6A 3K7 Canada

Supporting Information

ABSTRACT: The ternary clusters $(tmeda)_6Zn_{14-x}Mn_xS_{13}Cl_2$ (**1a−d**) and $(tmeda)_6Zn_{14-x}Mn_xSe_{13}Cl_2$ (**2a−d**), (tmeda = *N,N,N′,N′*-tetramethylethylenediamine; $x \approx 2-8$) and the binary clusters $(tmeda)_6Zn_{14}E_{13}Cl_2$ (E = S, **3**; Se, **4**;) have been isolated by reacting $(tmeda)Zn(ESiMe_3)_2$ with Mn(II) and Zn(II) salts. Single crystal X-ray analysis of the complexes confirms the presence of the six "$(tmeda)ZnE_2$" units as capping ligands that stabilize the clusters, and distorted tetrahedral geometry around the metal centers. Mn(II) is incorporated into the ZnE framework by substitution of Zn(II) ions in the cluster. The polynuclear complexes $(tmeda)_6Zn_{12.3}Mn_{1.7}S_{13}Cl_2$ **1a**, $(tmeda)_6Zn_{12.0}Mn_{2.0}Se_{13}Cl_2$ **2a**, and $(tmeda)_6Zn_{8.4}Mn_{5.6}Se_{13}Cl_2$ **2d** represent the first examples of "Mn/ZnE" clusters with structural characterization and indications of the local chemical environment of the Mn(II) ions. The incorporation of higher amounts of Mn into **1d** and **2d** has been confirmed by elemental analysis. Density functional theory (DFT) calculations indicate that replacement of Zn with Mn is perfectly feasible and at least partly allows for the identification of some sites preferred by the Mn(II) metals. These calculations, combined with luminescence studies, suggest a distribution of the Mn(II) in the clusters. The room temperature emission spectra of clusters **1c−d** display a significant red shift relative to the all zinc cluster **3**, with a peak maximum centered at 730 nm. Clusters **2c−d** display a peak maximum at 640 nm in their emission spectra.

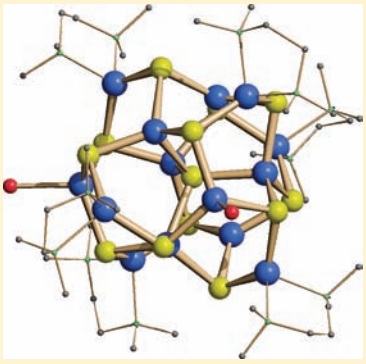

INTRODUCTION

Metal chalcogenolate complexes of the d-block metals with trimethylsilyl functionalities on the chalcogen centers have recently been utilized as precursors for the synthesis of ternary MM′E (E = S, Se, Te) nanoclusters. The preformed metal-chalcogen bond and high solubility of these complexes in common organic solvents, coupled with the reactivity of the $-ESiMe_3$ ligands toward ligand stabilized metal salts, makes them useful as precursors for the formation of M-E-M′ bonding interactions and entry into ternary d-block MM′E clusters and nanoclusters.[1−8] The coordination complex $(tmeda)Zn(SeSiMe_3)_2$ (tmeda = *N,N,N′,N′*-tetramethylethylenediamine) has been successfully utilized as a molecular precursors for the synthesis of the structurally characterized ternary nanocluster $[(tmeda\text{-}Zn)_5Cd_{11}Se_{13}(SePh)_6(THF)_2]$[4b] as well as for the preparation of ternary $Zn_xCd_{1-x}Se$ nanoparticles.[4c]

This demonstrated ability of metal-trimethylsilylchalcogenolate complexes as precursors for the controlled assembly of ternary cluster complexes has prompted us to develop this general synthetic route for the assembly of semiconducting systems containing the paramagnetic ions Mn(II). Such paramagnetic ions doped into nanoscale semiconductors (e.g., ZnE), often referred to as dilute magnetic semiconductors (DMS),[9] have attracted significant interest because of their potential applications as well as fundamental physical properties.[10−23] This is due to the unique size specific magnetic and optical properties that arises from the coexistence of the quantum confinement effect and its influence on the sp-d exchange interactions between magnetic ions and the semiconducting host. Mn(II) is by far the most commonly used dopant as paramagnetic ion, which acts both as luminescent center and localized spins in semiconductor nanocrystals.[24,25]

Recently, Eichhöfer and co-workers have prepared the mixed Mn−Cd−Se clusters $[Mn_6Cd_4Se_4(SePh)_{12}(PnPr_3)_4]$ and $[Cd_4Mn_4S(SePh)_{14}(PnPr_3)_2]$,[26] their report describing the first examples of such structurally characterized, ternary systems. Herein, we report the synthesis, structural characterization, and optical properties of the Mn(II) substituted ZnE nanoclusters $(tmeda)_6Zn_{14-x}Mn_xS_{13}Cl_2$ (**1a−d**) and $(tmeda)_6Zn_{14-x}Mn_xSe_{13}Cl_2$ (**2a−d**). The room temperature photoluminescence properties of these complexes are described and contrasted to those of the isostructural binary clusters, $(tmeda)_6Zn_{14}E_{13}Cl_2$ (E = S, **3**; E = Se, **4**).

EXPERIMENTAL SECTION

All experimental procedures were performed using standard double manifold Schlenk line techniques under an atmosphere of dried

Received: February 14, 2011
Published: February 22, 2012

   dx.doi.org/10.1021/ic200307g | *Inorg. Chem.* 2012, 51, 2747−2756

nitrogen gas or in nitrogen filled glove boxes. The nonchlorinated solvents (tetrahydrofuran, pentane) were dried and collected using a MBraun MB-SP Series solvent purification system with tandem activated alumina (tetrahydrofuran) and activated alumina/copper redox catalyst (pentane).[27] Dicholoromethane (CH_2Cl_2) was dried and distilled over P_2O_5. *N,N,N′,N′*-tetramethylethylenediamine was dried and distilled over CaH_2. Spectral grade solvents dimethylsulfoxide (DMSO) and CH_2Cl_2 were purchased from Caledon and dimethylformamide (DMF) from Fisher Chemicals. $MnCl_2$ and $Zn(OAc)_2$ were purchased from Aldrich in 98% and 99.99% purity, respectively, and used as supplied. The reagents $E(SiMe_3)_2$ (E = S, Se) were synthesized using literature procedures.[2,28] (tmeda)$Zn(ESiMe_3)_2$ (E = S, Se) was prepared following a previously published literature procedure.[29] Room temperature solution photoluminescence and photoluminescence excitation were measured on a Photon Technologies International Inc. Quantum Master equipped with a Xenon lamp. Room temperature UV−visible absorption spectra were recorded on a Varian Cary 300 spectrometer. Solution ^1H NMR spectra for **3** and **4** were recorded on a Varian Mercury 400 spectrometer with an operating frequency of 400.08 MHz and referenced externally to $SiMe_4$ and internally to the residual proton peak in CD_2Cl_2. Energy Dispersive X-ray (EDX) analysis on **1** and **2** were performed at Surface Science Western, London, Ontario. A Quartz XOne EDX analysis system coupled to a Leo 440 SEM equipped with a Gresham light element detector was used to obtain semiquantitative analysis of zinc and manganese. Elemental analysis was performed by Columbia Analytical Services (Tuscan, AZ, U.S.A.), Laboratoire d'Analyze Élementaire de l'Université de Montreal, Canada, or Guelph Chemical Laboratories Ltd., Canada. Metal analysis of **1** and **2** was performed using Inductively Coupled Plasma atomic emission spectroscopy (ICP-AES) by Columbia Analytical Services. Single crystals were examined under a microscope, selected, and dried under vacuum for 24 h prior to analysis. In some samples values obtained suggest partial retention of lattice solvent (CH_2Cl_2/pentane).

Single crystal X-ray data were collected on Bruker APEX-II CCD (**1a**, **2a**, **3**) and Enraf-Nonius Kappa-CCD (**2d**, **4**) diffractometers equipped with graphite-monochromated MoK_α (λ = 0.71073 Å) radiation. Highly solvated single crystals of the complexes were carefully selected, immersed in paraffin oil and mounted on a nylon loop. Crystals were placed immediately in a cold stream of N_2 to minimize desolvation. The structures were solved using direct methods and refined by the full-matrix least-squares procedure of SHELXTL.[30] All non-hydrogen cluster atoms were refined anisotropically, while hydrogen atoms were kept at their calculated distances and refined using a riding model. Partial site occupancy for Zn and Mn (see text) was evaluated by comparing respective thermal parameters. The site disorder was ultimately refined with common positional and thermal parameters for the two metals (EXYZ and EADP commands in SHELXTL, respectively). The refined Flack parameter for **2d** was −0.009(18). Quantum chemical calculations were carried out at the at density functional theory (DFT) level (program system TURBOMOLE,[31] BP86,[32] and B3LYP[33] functionals, def-SV(P) bases and respective Coulomb fitting bases[34]).

Synthesis of (tmeda)$_6$Zn$_{12.3}$Mn$_{1.7}$S$_{13}$Cl$_2$ 1a. $MnCl_2$ (0.022 g, 0.174 mmol) was dissolved in 5 mL of CH_2Cl_2 by adding tmeda (0.04 mL, 0.268 mmol), and the pale orange solution was cooled to −75 °C. $Zn(OAc)_2$ (0.096 g, 0.523 mmol) was dissolved in 5 mL of CH_2Cl_2 by adding tmeda (0.12 mL, 0.805 mmol), and the clear solution was cooled to −75 °C. These two solutions were then added to previously prepared colorless solution of (tmeda)$Zn(SSiMe_3)_2$ (0.274 g, 0.699 mmol) in 10 mL of CH_2Cl_2 at −75 °C. The very pale yellow solution was left stirring overnight with the temperature increasing slowly to room temperature. Almost colorless crystals were obtained after a few days by the reduction of solvent volume by half and slow diffusion of pentane at room temperature. Yield: 0.093 g (44%). Anal. Calcd for $C_{36}H_{96}Cl_2N_{12}S_{13}Zn_{12.3}Mn_{1.7}$: C, 20.80%; H, 4.65%. Found: C, 20.99%; H, 4.85%.

Synthesis of (tmeda)$_6$Zn$_{10.9}$Mn$_{3.1}$S$_{13}$Cl$_2$ 1b. $MnCl_2$ (0.068 g, 0.540 mmol) was dissolved in 5 mL of CH_2Cl_2 by adding tmeda (0.12 mL, 0.805 mmol), and the pale orange solution was cooled to −75 °C. $Zn(OAc)_2$ (0.098 g, 0.534 mmol) was dissolved in 5 mL of CH_2Cl_2 by adding tmeda (0.12 mL, 0.805 mmol), and the clear solution was cooled to −75 °C. These two solutions were then added to previously prepared colorless solution of (tmeda)$Zn(SSiMe_3)_2$ (0.420 g, 1.07 mmol) in 10 mL of CH_2Cl_2 at −75 °C. Analogous experimental procedure as **1a**, afforded pale orange crystals of **1b**. Yield: 0.140 g (39%). Anal. Calcd for $C_{36}H_{96}Cl_2N_{12}S_{13}Zn_{10.9}Mn_{3.1}$: C, 20.90%; H, 4.68%. Found: C, 20.97%; H, 4.84%.

Synthesis of (tmeda)$_6$Zn$_{10.0}$Mn$_{4.0}$S$_{13}$Cl$_2$ 1c. $MnCl_2$ (0.056 g, 0.445 mmol) was dissolved in 5 mL of CH_2Cl_2 by adding tmeda (0.1 mL, 0.671 mmol), and the pale orange solution was cooled to −75 °C. $Zn(OAc)_2$ (0.035 g, 0.191 mmol) was dissolved in 5 mL of CH_2Cl_2 by adding tmeda (0.04 mL, 0.268 mmol), and the clear solution was cooled to −75 °C. These two solutions were then added to previously prepared colorless solution of (tmeda)$Zn(SSiMe_3)_2$ (0.250 g, 0.638 mmol) in 10 mL of CH_2Cl_2 at −75 °C. Analogous experimental procedure as **1a**, afforded orange crystals of **1c**. Yield: 0.0.090 g (39%). Anal. Calcd for $C_{36}H_{96}Cl_2N_{12}S_{13}Zn_{10.0}Mn_{4.0}$: C, 21.00%; H, 4.70%. Found: C, 21.67%; H, 5.10%.

Synthesis of (tmeda)$_6$Zn$_{6.2}$Mn$_{7.8}$S$_{13}$Cl$_2$ 1d. The synthesis was carried out in a similar manner as **1a**, with $MnCl_2$ (0.120 g, 0.953 mmol), tmeda (0.22 mL, 1.50 mmol), and (tmeda)$Zn(SSiMe_3)_2$ (0.360 g, 0.918 mmol). Orange crystals were obtained by the reduction of solvent volume by half and slow diffusion of pentane at room temperature after a few days. Yield: 0.125 g (50%). Anal. Calcd for $C_{36}H_{96}Cl_2N_{12}S_{13}Zn_{6.2}Mn_{7.8}$: C, 21.44%; H, 4.80%. Found: C, 21.54%; H, 4.61%. Unit cell parameters of single crystals matched those for **1a**.

Synthesis of (tmeda)$_6$Zn$_{12.0}$Mn$_{2.0}$Se$_{13}$Cl$_2$ 2a. $MnCl_2$ (0.026 g, 0.206 mmol) was dissolved in 5 mL of CH_2Cl_2 by adding tmeda (0.05 mL, 0.336 mmol), and the pale orange solution was cooled to −75 °C. $Zn(OAc)_2$ (0.113 g, 0.616 mmol) was dissolved in 5 mL of CH_2Cl_2 by adding tmeda (0.14 mL, 0.939 mmol), and the clear solution was cooled to −75 °C. These two solutions were then added to previously prepared solution of (tmeda)$Zn(SeSiMe_3)_2$ (0.400 g, 0.823 mmol) in 10 mL of CH_2Cl_2 at −75 °C. The pale orange solution was left stirring overnight letting the temperature increase slowly to room temperature. Almost colorless crystals were obtained by the reduction of solvent volume and slow diffusion of pentane at room temperature after a few days. Yield: 0.120 g (42%). Anal. Calcd for $C_{36}H_{96}Cl_2N_{12}Se_{13}Zn_{12}Mn_2$: C, 16.08%; H, 3.60%. Found: C, 15.17%; H, 3.55%.

Synthesis of (tmeda)$_6$Zn$_{10.8}$Mn$_{3.2}$Se$_{13}$Cl$_2$ 2b. The synthesis was carried out in a similar manner as for **2a**. $MnCl_2$ (0.047 g, 0.373 mmol) was dissolved in 5 mL of CH_2Cl_2 by adding tmeda (0.08 mL, 0.537 mmol), and the orange solution was cooled to −75 °C. $Zn(OAc)_2$ (0.068 g, 0.371 mmol) was dissolved in 5 mL of CH_2Cl_2 by adding tmeda (0.08 mL, 0.536 mmol), and the clear solution was cooled to −75 °C. These solutions were then added to a previously prepared solution of (tmeda)$Zn(SeSiMe_3)_2$ (0.360 g, 0.740 mmol) in 10 mL of CH_2Cl_2 at −75 °C. Analogous experimental procedure as for **2a** afforded pale orange crystals Yield: 0.137 g (44%). Anal. Calcd for $C_{36}H_{96}Cl_2N_{12}Se_{13}Zn_{10.8}Mn_{3.2}$: C, 16.14%; H, 3.61%. Found: C, 15.61%; H, 3.63%.

Synthesis of (tmeda)$_6$Zn$_{10.7}$Mn$_{3.3}$Se$_{13}$Cl$_2$ 2c. $MnCl_2$ (0.092 g, 0.731 mmol) was dissolved in 10 mL of CH_2Cl_2 by adding tmeda (0.16 mL, 1.07 mmol), and the orange solution was cooled to −75 °C. $Zn(OAc)_2$ (0.058 g, 0.316 mmol) was dissolved in 5 mL of CH_2Cl_2 by adding tmeda (0.07 mL, 0.470 mmol), and the clear solution was cooled to −75 °C. These solutions were then added to a previously prepared solution of (tmeda)$Zn(SeSiMe_3)_2$ (0.506 g, 1.04 mmol) in 10 mL of CH_2Cl_2 at −75 °C. Analogous crystallization procedure as for **2a** afforded orange crystals. Yield: 0.198 g (33%). Anal. Calcd for $C_{36}H_{96}Cl_2N_{12}Se_{13}Zn_{10.7}Mn_{3.3}$: C, 16.14%; H, 3.61%. Found: C 16.88% and H 4.12%

Synthesis of (tmeda)$_6$Zn$_{8.4}$Mn$_{5.6}$Se$_{13}$Cl$_2$ 2d. $MnCl_2$ (0.115 g, 0.913 mmol) was dissolved in 10 mL of CH_2Cl_2 by adding tmeda (0.20 mL, 1.50 mmol), and the orange solution was cooled to −75 °C. This solution was then added to a previously prepared solution of (tmeda)$Zn(SeSiMe_3)_2$ (0.435 g, 0.895 mmol) in 10 mL of CH_2Cl_2 tlsb=-0.01w?>at −75 °C. Analogous crystallization procedure as **2a**, afforded orange crystals. Yield: 0.180 g (58%). Anal. Calcd for

dx.doi.org/10.1021/ic200307g | *Inorg. Chem.* 2012, 51, 2747−2756

Table 1. Crystallographic Data

	1a	2a	2d	3	4
chemical formula	$C_{36}H_{96}Cl_2N_{12}S_{13}Mn_1Zn_{13}\cdot(CH_2Cl_2)_9$	$C_{36}H_{96}Cl_2N_{12}Se_{13}Mn_1Zn_{13}\cdot(CH_2Cl_2)_9$	$C_{36}H_{96}Cl_2N_{12}Se_{13}Mn_{5.60}Zn_{8.40}\cdot(CH_2Cl_2)_{3.5}$	$C_{36}H_{96}Cl_2N_{12}S_{13}Zn_{14}\cdot(CH_2Cl_2)_9$	$C_{36}H_{96}Cl_2N_{12}Se_{13}Zn_{14}\cdot(CH_2Cl_2)_9$
Fw	2854.01	3459.68	2948.64	2864.44	3474.43
space group	$P\bar{1}$	$P\bar{1}$	$P3(1)21$	$P\bar{1}$	$P\bar{1}$
temp (K)	150(2)	150(2)	150(2)	150(2)	150(2)
a (Å)	13.5003(7)	13.5535(7)	25.5250(3)	13.4610(19)	13.5553(2)
b (Å)	13.7288(7)	13.7519(7)	25.5250(3)	13.7110(19)	13.7348(2)
c (Å)	28.6237(14)	28.9793(15)	27.9532(5)	28.542(4)	28.9568(4)
α (deg)	99.918(2)	99.455(2)	90	100.000(6)	99.4740(7)
β (deg)	93.060(3)	92.747(2)	90	93.060(7)	92.7150(7)
γ (deg)	93.835(2)	93.280(2)	120	93.710(8)	93.1470(8)
V (Å^3)	5202.8(5)	5310.2(5)	15772(4)	5165.7(12)	5300.89(13)
μ (mm^{-1})	3.863	7.985	7.282	4.001	8.106
Z	2	2	6	2	2
ρ (g cm^{-3})	1.822	2.164	1.863	1.842	2.171
data/params	13914/937	19534/945	11601/794	22747/951	19045/958
R_1 [$I > 2\sigma(I)$]	0.0520	0.0583	0.0625	0.0431	0.0629
wR_2 [$I > 2\sigma(I)$]	0.1082	0.1364	0.1553	0.1051	0.1856
Flack parameter			−0.009(18)		

$C_{36}H_{96}Cl_2N_{12}Se_{13}Zn_{8.4}Mn_{5.6}$: C, 16.33%; H, 3.66%. Found: C, 15.61% and H 3.63%.

Synthesis of (tmeda)$_6$Zn$_{14}$S$_{13}$Cl$_2$ 3. $Zn(OAc)_2$ (0.105 g, 0.57 mmol) was dissolved in 10 mL of CH_2Cl_2 by adding tmeda (0.13 mL, 1.50 mmol), and the colorless solution was cooled to −75 °C. This solution was then added to a previously prepared solution of $(tmeda)Zn(SSiMe_3)_2$ (0.215 g, 0.55 mmol) in 10 mL of CH_2Cl_2 at −75 °C. The colorless solution was left stirring overnight allowing the temperature to increase slowly to room temperature. Colorless block crystals were obtained by the reduction of solvent volume by half and slow diffusion of pentane at room temperature after a few days. Yield: 0.080 g (45%). Anal. Calcd for $C_{36}H_{96}Cl_2N_{12}S_{13}Zn_{14}$: C, 20.59%; H, 4.61%. Found: C, 19.47%; H, 4.84%.

Synthesis of (tmeda)$_6$Zn$_{14}$Se$_{13}$Cl$_2$ 4. $Zn(OAc)_2$ (0.140 g, 0.76 mmol) was dissolved in 10 mL of CH_2Cl_2 by adding tmeda (0.17 mL, 1.50 mmol), and the colorless solution was cooled to −75 °C. This solution was then added to a previously prepared pale yellow solution of $(tmeda)Zn(SeSiMe_3)_2$ (0.369 g, 0.76 mmol) in 10 mL of CH_2Cl_2 at −75 °C. Analogous crystallization procedure as for **3** afforded colorless, block-like crystals. Yield: 0.125 g (40%). Anal. Calcd for $C_{36}H_{96}Cl_2N_{12}Se_{13}Zn_{14}$: C, 15.95%; H, 3.57%. Found: C, 16.80%; H, 3.29%.

RESULTS AND DISCUSSION

Synthesis and Characterization of Chalcogenide Complexes. The reaction of the chalcogenolate coordination complex $(tmeda)Zn(ESiMe_3)_2$ with tmeda solubilized metal salts afforded the isolation of the ternary clusters (**1a**−**d**, **2a**−**d**) as well as the binary clusters **3** and **4** (eq 1) as the only products isolated after crystallization.

$$\begin{aligned} &13(tmeda)Zn(ESiMe_3)_2 + 2x(tmeda)MnCl_2 \\ &\quad + (15 - 2x)(tmeda)Zn(OAc)_2 \\ &\quad \rightarrow 2[(tmeda)_6Zn_{14-x}M_xE_{13}Cl_2] \\ &\quad + 26Cl/OAcSiMe_3 + 23.5tmeda \\ &\quad (x = 0,\ 1.75,\ 3.5,\ 4.9,\ 7.5) \end{aligned} \quad (1)$$

The generation of $ClSiMe_3$ and/or $AcOSiMe_3$ is the driving force for these reactions, which leads to the formation of metal-chalcogen bonding interactions. Exploiting the reactivity of the zinc chalcogenolate precursor and the versatility of the reaction eq 1, we were able to synthesize ternary clusters with some control over the amount of Mn(II) introduced. Chalcogenide (E^{2-}) ligands tend to adopt bridging coordination modes because of the high polarizabilty of these centers, which often results in the formation of polynuclear species.[7] The isolation of these manganese containing "ZnE" clusters with varying amounts of "dopant", provides an opportunity to study the effect of Mn(II) concentration on the photoluminescence properties of these systems. Single-crystal X-ray diffraction data were collected for complexes **1a**, **2a**, **2d**, **3**, and **4**, and cell constants were recorded for complexes **1b**, **1d**, and **2b**. A summary of the crystallographic and refinement data for all complexes is listed in Table 1.

The common structural feature prevalent in the clusters is the presence of a central core that consists of a "$M_{14}E_{13}$" unit that is stabilized by six tmeda and two terminal chloride ligands (Figure 1 and Figure 2). The chelating tmeda ligands are coordinated to six zinc atoms that are present on the surface of the cluster, thus preventing further condensation of the cluster into bulk solids. This arrangement has previously been observed in the zinc-telluride cluster $(tmeda)_6Zn_{14}Te_{13}Cl_2$,[35] and a related $M_{14}E_{13}$ frame has also been displayed with the ternary copper−indium-chalcogenides $[Cu_6In_8E_{13}Cl_4(PR_3)_{12}]$ (E = S, Se; R = alkyl).[1b,6d]

The binary clusters $(tmeda)_6Zn_{14}S_{13}Cl_2$ **3** and $(tmeda)_6Zn_{14}Se_{13}Cl_2$ **4** can be prepared from a combination of $Zn(OAc)_2$ with the zinc chalcogenolates $(tmeda)Zn(SSiMe_3)_2$ and $(tmeda)Zn(SeSiMe_3)_2$, respectively, as outlined in eq 1. The solid state molecular structure obtained from single crystal X-ray diffraction is shown in Figure 1 for the sulfide complex $(tmeda)_6Zn_{14}S_{13}Cl_2$ **3**. Cluster **3** crystallizes in the triclinic space group, $P\bar{1}$ with Z = 2 and there are nine CH_2Cl_2 solvent molecules present in the asymmetric unit. The isostructural and isomorphous selenide complex **4** was also isolated in the form of single crystals, and its structure was determined. The molecular structure of both ternary (vide infra) and binary clusters shows that the zinc chalcogenolate precursors successfully deliver "ZnE_2" into the cluster core and act as a source of six "$(tmeda)ZnE_2$" units that stabilize the polyhedron. The geometry around the Zn centers is distorted tetrahedral.

dx.doi.org/10.1021/ic200307g | Inorg. Chem. 2012, 51, 2747−2756

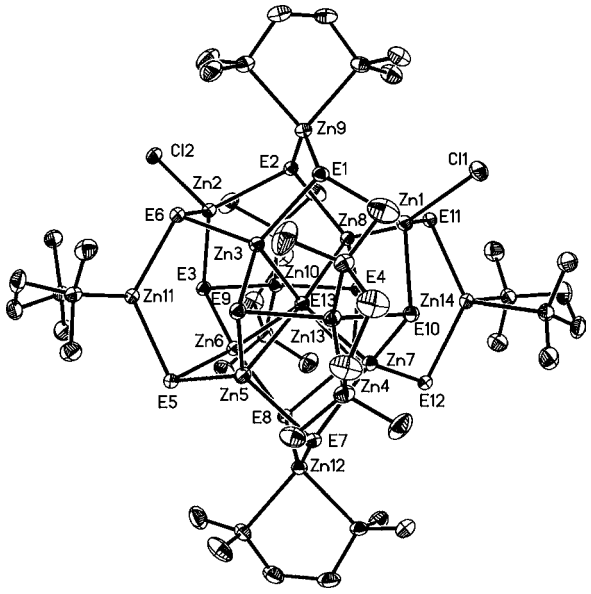

Figure 1. Molecular structure of $(tmeda)_6Zn_{14}E_{13}Cl_2$ (E = S (illustrated), Se). Thermal ellipsoids are drawn at the 45% probability level. Hydrogen atoms are omitted for clarity.

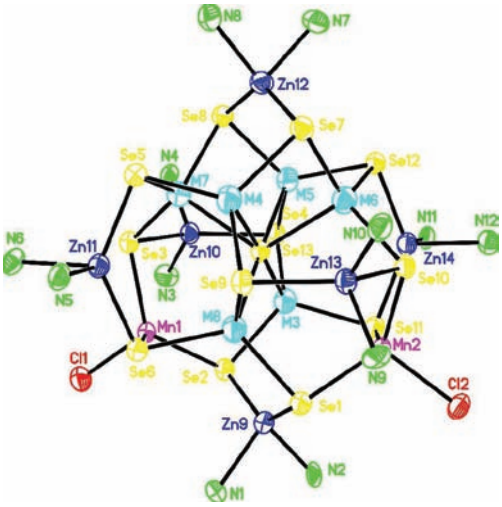

Figure 2. Molecular structure of $(tmeda)_6Zn_{10}Mn_4Se_{13}Cl_2$ **2d** (45% probability level; H and C atoms omitted). Blue, Zn; violet, Mn; yellow, Se; green, N; red, Cl. Cyano colored metal sites represent those with refined partial occupancy of Zn and Mn in **2d**.

Interestingly, there are two chloride ligands bonded to two Zn(II) at the surface of the cluster (Figure 1). Although the source of the chloride ion must be solvent, the syntheses and yields of **3** and **4** using $Zn(OAc)_2$ are entirely reproducible. Each zinc is four coordinate, with Zn9–Zn14 bonded to a bidentate tmeda ligand and two chalcogenide ions, Zn1 and Zn2 each bonded to one Cl^- and three E^{2-}. There are six interstitial zinc(II) tetrahedrally bonded to four sulfur (**3**) or selenium (**4**) centers. Notably, the fourth metal-chalcogen contact to the central E(13) for the sites Zn(4) and Zn(5) is markedly longer (~0.5 Å) than the other three (Table 2). This point is discussed further when examining the distribution of Mn in the mixed-metal clusters via quantum chemical calculations. The E_{13} chalcogenide framework in the complexes consists of a nonbonded E_{12} icosahedral arrangement (E1-E12) around a central chalcogen. Summaries of the bond distances and angles for **3** and **4** are listed in Table 2 and Table 3, respectively. Each of the chalcogens bridges three zinc centers with the exception of the central ligand, which is within

Table 2. Selected Bond Distances (Å) of Complexes 3 and 4

	3 (E = S)	**4** (E = Se)
Zn(1)–E(1)	2.3485(11)	2.4709(11)
Zn(1)–E(10)	2.3573(11)	2.4782(11)
Zn(1)–E(11)	2.3534(11)	2.4529(11)
Zn(1)–Cl(1)	2.3663(11)	2.343(2)
Zn(2)–E(2)	2.3565(11)	2.4658(12)
Zn(2)–E(3)	2.3673(11)	2.4703(11)
Zn(2)–E(6)	2.3470(11)	2.4665(11)
Zn(2)–Cl(2)	2.3570(11)	2.358(2)
Zn(3)–E(1)	2.3245(11)	2.4198(11)
Zn(3)–E(6)	2.3248(11)	2.4471(11)
Zn(3)–E(9)	2.4039(11)	2.4929(11)
Zn(3)–E(13)	2.4628(10)	2.5665(11)
Zn(4)–E(4)	2.2851(11)	2.4099(11)
Zn(4)–E(8)	2.2999(11)	2.4120(11)
Zn(4)–E(12)	2.2923(11)	2.4007(12)
Zn(4)–E(13)	2.7974(11)	2.9278(6)
Zn(5)–E(5)	2.2908(11)	2.4094(12)
Zn(5)–E(7)	2.2951(11)	2.4172(11)
Zn(5)–E(9)	2.2979(11)	2.3977(11)
Zn(5)–S(13)	2.8367(11)	2.8930)11)
Zn(6)–E(3)	2.3146(11)	2.4249(11)
Zn(6)–E(5)	2.3583(11)	2.4644(11)
Zn(6)–E(8)	2.4108(10)	2.4930(11)
Zn(6)–E(13)	2.4376(10)	2.5287(11)
Zn(7)–E(7)	2.3782(11)	2.5197(11)
Zn(7)–E(10)	2.3172(11)	2.4254(11)
Zn(7)–E(12)	2.3592(11)	2.4681(11)
Zn(7)–E(13)	2.4351(10)	2.5302(11)
Zn(8)–E(2)	2.3142(10)	2.4346(11)
Zn(8)–E(4)	2.3893(11)	2.5138(11)
Zn(8)–E(11)	2.3399(10)	2.4286(11)
Zn(8)–E(13)	2.4623(11)	2.5635(11)
Zn(9)–N(1)	2.178(3)	2.175(6)
Zn(9)–N(2)	2.170(3)	2.182(6)
Zn(9)–E(1)	2.2720(11)	2.3892(11)
Zn(9)–E(2)	2.2794(11)	2.3901(11)
Zn(10)–E(3)	2.2725(11)	2.3884(11)
Zn(10)–E(4)	2.2793(11)	2.4011(12)
Zn(10)–N(3)	2.159(4)	2.156(6)
Zn(10)–N(4)	2.175(3)	2.182(7)
Zn(11)–E(5)	2.3066(10)	2.4059(12)
Zn(11)–E(6)	2.2732(11)	2.3805(11)
Zn(11)–N(5)	2.121(3)	2.171(6)
Zn(11)–N(6)	2.168(3)	2.164(6)
Zn(12)–E(7)	2.2811(11)	2.4013(11)
Zn(12)–E(8)	2.2868(11)	2.3946(11)
Zn(12)–N(7)	2.152(3)	2.157(6)
Zn(12)–N(8)	2.169(3)	2.149(6)
Zn(13)–E(9)	2.2802(11)	2.3998(11)
Zn(13)–E(10)	2.2771(11)	2.3843(11)
Zn(13)–N(9)	2.161(3)	2.165(7)
Zn(13)–N(10)	2.182(3)	2.182(6)
Zn(14)–E(11)	2.2686(10)	2.3866(11)
Zn(14)–E(12)	2.2922(11)	2.4214(11)
Zn(14)–N(11)	2.179(3)	2.177(6)
Zn(14)–N(12)	2.154(3)	2.135(7)

dx.doi.org/10.1021/ic200307g | Inorg. Chem. 2012, 51, 2747–2756

bonding distance to six metals albeit with four shorter (~2.4 Å, **3**; 2.5 Å, **4**) and two longer (~2.6 Å, **3**; ~2.9 Å, **4**) contacts.

Table 3. Selected Bond Angles (deg) of Complexes 3 and 4

	3 (E = S)	4 (E = Se)
E(1)−Zn(1)−E(11)	114.03(4)	112.28(4)
E(1)−Zn(1)−E(10)	114.01(4)	115.11(4)
E(11)−Zn(1)−E(10)	115.64(4)	114.96(4)
E(1)−Zn(1)−Cl(1)	105.46(4)	103.49(6)
E(10)−Zn(1)−Cl(1)	102.40(4)	107.31(6)
E(11)−Zn(1)−Cl(1)	103.30(4)	102.10(6)
E(4)−Zn(4)−E(12)	118.67(4)	119.05(4)
E(4)−Zn(4)−E(8)	119.84(4)	118.49(4)
E(12)−Zn(4)−E(8)	120.06(4)	120.47(4)
E(4)−Zn(4)−E(13)	94.23(3)	95.06(4)
E(12)−Zn(4)−E(13)	94.05(3)	95.03(3)
E(8)−Zn(4)−E(13)	93.63(3)	93.99(4)
E(3)−Zn(6)−E(5)	116.41(4)	115.26(4)
E(3)−Zn(6)−E(8)	113.98(4)	114.42(4)
E(5)−Zn(6)−E(8)	112.81(4)	112.60(4)
E(3)−Zn(6)−E(13)	107.60(4)	106.65(4)
E(5)−Zn(6)−E(13)	103.34(4)	103.56(4)
E(8)−Zn(6)−E(13)	100.63(4)	102.66(4)
E(10)−Zn(7)−E(12)	116.84(4)	115.56(4)
E(10)−Zn(7)−E(7)	114.45(4)	113.35(4)
E(12)−Zn(7)−E(7)	112.91(4)	112.34(4)
E(10)−Zn(7)−E(13)	106.75(4)	107.87(4)
E(12)−Zn(7)−E(13)	102.52(4)	104.29(4)
E(7)−Zn(7)−E(13)	101.02(4)	101.92(4)
N(3)−Zn(10)−N(4)	84.29(13)	84.7(3)
N(3)−Zn(10)−E(3)	114.86(10)	110.3(2)
N(4)−Zn(10)−E(3)	106.53(10)	107.26(19)
N(4)−Zn(10)−E(4)	109.74(10)	110.48(19)
E(3)−Zn(10)−E(4)	128.20(4)	127.67(4)
N(7)−Zn(12)−N(8)	84.75(13)	84.9(3)
N(7)−Zn(12)−E(7)	112.12(10)	111.84(17)
N(8)−Zn(12)−E(7)	105.75(9)	105.44(19)
N(7)−Zn(12)−E(8)	105.74(10)	105.71(18)
N(8)−Zn(12)−E(8)	112.22(10)	111.97(18)
E(7)−Zn(12)−E(8)	127.91(4)	128.46(4)
N(12)−Zn(14)−N(11)	84.41(13)	84.4(2)
N(12)−Zn(14)−E(11)	113.25(10)	112.25(18)
N(11)−Zn(14)−E(11)	109.67(10)	105.78(17)
N(12)−Zn(14)−E(12)	105.72(10)	107.65(17)
N(11)−Zn(14)−E(12)	108.59(10)	112.09(17)
E(11)−Zn(14)−E(12)	126.95(4)	126.66(4)
Zn(7)−E(13)−Zn(6)	115.70(4)	114.36(4)
Zn(7)−E(13)−Zn(8)	109.90(4)	108.68(4)
Zn(3)−E(13)−Zn(8)	102.83(4)	103.97(3)
Zn(3)−E(13)−Zn(4)	175.90(4)	176.11(4)
Zn(8)−E(13)−Zn(4)	73.07(3)	72.18(3)
Zn(8)−E(13)−Zn(5)	175.09(4)	176.39(4)
Zn(4)−E(13)−Zn(5)	111.81(3)	111.40(3)

The strategy of using the reagents (tmeda)$Zn(SSiMe_3)_2$ and (tmeda)$Zn(SeSiMe_3)_2$ for the preparation of the all Zn complexes suggested that mixed metal species could also be prepared by reacting them with a different metal salt. In this vein, adding a defined ratio of Mn(II):Zn(II) to solutions of (tmeda)$Zn(ESiMe_3)_2$ led to the formation of similar frameworks, but with varying amounts of manganese present in the clusters as determined by elemental analysis and changes in the luminescence properties, and supported by single crystal X-ray diffraction.

Table 4 lists the atomic ratio of Zn:Mn found in clusters **1**-**2** as determined via inductively coupled plasma atomic emission spectroscopy (ICP-AES). The observed values indicate that the ratio between the two metals generally matches that introduced into the reaction mixtures (eq 1), with the exception of **2c** and **2d**, where the Mn content in the clusters are both lower than were introduced in the reaction scheme.

Table 4. Atomic Ratio of Zinc and Manganese in Clusters 1a−d and 2a−d As Determined by ICP-AES

	1a	1b	1c	1d	2a	2b	2c	2d
Mn	1.7	3.1	4.0	7.8	2.0	3.2	3.3	5.4
Zn	12.3	10.9	10.0	6.2	12.0	10.8	10.7	8.6

Single crystal X-ray analysis of the mixed metal clusters confirmed that, as observed for **3** and **4**, all of the metal centers adopt distorted tetrahedral geometries. The slight differences in the scattering power of Zn and Mn together with site disorder of the Mn(II) make it difficult to model the occupancies accurately from the diffraction data. However, satisfactory refinement was achieved with the Zn ions occupying the six surface sites ligated by the tmeda ligands (Zn9−Zn14); the two metal sites bonded to the terminal chloride ions were best refined with full occupancy by manganese (Mn1 and Mn2) when the Mn content was greater than 2 atoms per cluster. Refinement of the crystallographic data for **1a** (S) and **2a** (Se) was satisfactorily completed with the two Mn centers with occupancy 0.5 at the two M-Cl sites (Figure 2) but the site specific location of remaining Mn(II) ions is difficult to ascertain from the crystallographic data and the similar scattering power of Zn(II) and Mn(II). The listed Mn:Zn stoichiometries in Table 1, which can differ from those in Table 4, refer to the crystallographic models that were refined for the clusters. The site occupancies are supported by the calculated structures for the mixed metal species (vide infra). Overall, the local coordination geometries of the individual metal sites do not change drastically from those observed in **3** and **4** with increasing Mn content, reflecting the small differences in the ionic radii for the two four-coordinate metals (0.74 Å Zn(II); 0.80 Å Mn(II) high spin).[36] The overall sizes of the Mn−Zn-E cluster cores are approximately 9 Å × 9 Å × 9 Å.

The cluster $(tmeda)_6Zn_{8.4}Mn_{5.6}Se_{13}Cl_2$ **2d** crystallizes in the trigonal space group *P*3(2)21 with 3.5 molecules of CH_2Cl_2. Selected bond distances for **2d** are summarized in Supporting Information, Table S1. The two metal sites ligated to Cl were refined with full occupancy of Mn and, excluding the six tmeda ligated Zn sites, the remaining six metal positions present in the cluster core of **2d** were satisfactorily refined with partial occupancy of both zinc and manganese. The molecular structure of **2d** is shown in Figure 2.

The average Mn−Se bond distance is 2.544(8) Å. The Mn−Cl and Mn−Se bond distances are similar to those observed in the adamantoid complex $[Mn_4(SeiPr)_6)Br_4]^{2-}$.[37] The Mn−Se bond distances are also comparable to those observed in $[Mn_{32}Se_{14}(SePh)_{36}(P^nPr_3)_4]$ and $[Mn_8Se(SePh)_{16}]^{2-}$.[38] Refined Zn−Se bond distances are comparable with those observed in **3** and **4** and to those previously reported in $[Zn_{10}S_7(SO_4)_3(py)_9]$[39] (py = pyridine), $[Zn_{10}S_4(SEt)_{12}(L)_4]$,[40] $[Zn_8Se(SePh)_{12}Cl_4]^{2-}$,[41] and $[(tmeda)_5Zn_5Cd_{11}Se_{13}(SePh)_6(thf)_2]$.[4b]

dx.doi.org/10.1021/ic200307g | Inorg. Chem. 2012, 51, 2747−2756

Photoluminescence Properties. Room temperature (solution) UV−visible absorption, photoluminescence (PL), and photoluminescence excitation (PLE) spectra were recorded for the clusters. Figure 3 shows the PL, PLE, and absorption

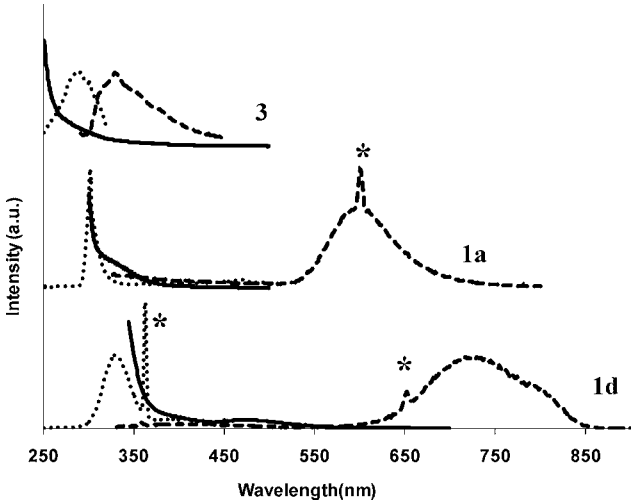

Figure 3. Normalized room temperature absorption (solid lines) and PL (dashed lines) spectra of **3**, **1a**, and **1d** in DCM, DMSO, and DMF, respectively. The * denote harmonic vibration and/or solvent peaks. PLE (dotted lines) were recorded using an excitation energy at the observed PL maximum.

spectra of $(tmeda)_6Zn_{14}S_{13}Cl_2$ **3**, $(tmeda)_6Zn_{12.3}Mn_{1.7}S_{13}Cl_2$ **1a**, and $(tmeda)_6Zn_{6.2}Mn_{7.8}S_{13}Cl_2$ **1d**. Spectra for $(tmeda)_6Zn_{10.9}Mn_{3.1}S_{13}Cl_2$ **1b** and $(tmeda)_6Zn_{10.0}Mn_{4.0}S_{13}Cl_2$ **1c** are illustrated in Supporting Information, Figure S3. The maximum PL emission band for the binary ZnS cluster **3** is observed at 321 nm. Upon incorporation of ∼2 Mn(II) to yield the heterometallic cluster **1a**, a drastically different PL emission spectrum is observed, as shown in Figure 3. The complete disappearance of the "band-edge" emission peak from **3** is accompanied by a large Stokes shift with a PL peak maximum observed at 590 nm. When the amount of Mn was increased to yield cluster **1b**, the maximum PL emission is observed at ∼600 nm. The emission at ∼600 nm observed in **1a** and **1b** is no longer observed when the amount of Mn incorporated into the cluster is increased further. For **1c** and **1d** a single PL emission maximum is observed ∼730 nm for both compounds. At ambient temperatures, these emissions are very weak, as has been documented for the ternary Cd-Mn-E (E = S, Se) clusters.[26] For each manganese containing complex, weak absorption transitions are observed centered around ∼450 nm, consistent with d-d transitions of the tetrahedrally coordinated d^5 metals in Mn−Se clusters.[26,38]

Figure 4 shows the room temperature (solution) UV−visible absorption, PL, and PLE spectra of clusters $(tmeda)_6Zn_{14}Se_{13}Cl_2$ **4**, $(tmeda)_6Zn_{12.0}Mn_{2.0}Se_{13}Cl_2$ **2a**, and $(tmeda)_6Zn_{8.4}Mn_{5.6}Se_{13}Cl_2$ **2d**. Spectra for **2b** and **2c** are illustrated in Supporting Information, Figure S4. The PL spectra of the all Zn cluster **4** display a weak maximum at 450 nm when irradiated at 375 nm. However, the emission profiles for the ZnSe clusters incorporating Mn(II) are again markedly different. A broad PL emission peak centered at 620 nm is observed for cluster **2a** with a smaller shoulder observed at 560 nm. The large Stokes shift observed in **2a** as compared to very small shift displayed by the all Zn cluster **4** provide

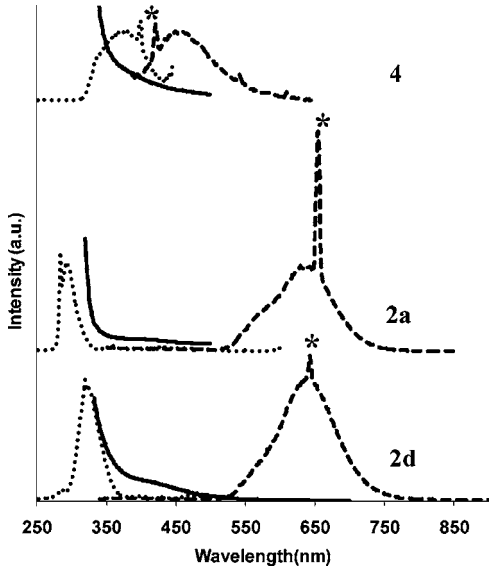

Figure 4. Normalized room temperature UV−visible (solid lines) and PL (dashed lines) spectra of **4**, and **2a**, and **2d** in DMSO, DCM, and DCM, respectively. The * denote harmonic vibration and/or solvent peaks. PLE (dotted lines) were recorded using an excitation energy at the observed PL maximum.

evidence in support of successful incorporation of Mn(II) into the ZnSe framework. As observed for the sulfide clusters **1a-1d**, the PL emission profiles of Mn containing ZnSe clusters change with the incorporation of higher amounts of manganese. Thus for complexes **2c** and **2d**, the shoulder observed at 560 nm in **2a** and **2b** is no longer observed, with the emission at 640 nm being dominant. The origin of two emissions is not certain at present, but it likely reflects a distribution of clusters $(tmeda)_6Zn_{14-x}Mn_xSe_{13}Cl_2$ in which the number of Mn(II) in the individual clusters is either lower (560 nm) or higher (640 nm).

The PL emission energies observed for **1c**, **1d**, and **2a**−**d** are significantly red-shifted compared to those reported for ZnE nanoparticles with low concentrations of Mn(II) dopants (dilute magnetic semiconductors, DMS). It is well established that incorporation of Mn(II) into a ZnE nanoparticle host results in the efficient energy transfer into the electronic state of Mn(II), which undergoes atomic like transition from the lowest excited state ($^4T_1$) to the ground state ($^6A_1$), with a characteristic orange luminescence maximum at about 590 nm.[25,42] In contrast, the emission energies for clusters with high amounts of manganese, namely, $[Cd_4Mn_6Se_4(SePh)_{12}(PPr_3)_4]$ and $[Cd_4Mn_4S(SePh)_{14}(PPr_3)_2]$, are observed at 780 and 725 nm, respectively.[26] The PL emission observed here in the yellow-orange region of visible spectrum for clusters with a small number (2−3) of Mn(II) centers (**1a**−**b**, **2a**−**b**) have emission energies similar to the electronic transition from $^6A_1 \leftarrow {}^4T_1$ observed in DMS systems. Increasing the number of manganese centers in the clusters **1** and **2** results in a shift of their emission energies to 730 nm (sulfide; **1c**−**d**) and 640 nm (selenide; **2c**−**d**). This energy shift from commonly observed yellow-orange to red region of the spectrum could be due to the separation of the "ZnMnE" clusters into separate "ZnE" and "MnE" species. However solid-state PL spectra (as nujol mulls between quartz plates) of **1a** (Figure 5) are similar to those observed in the solution state. For **2a**, the relative intensities of the two emissions observed is inverted; this may indicate a redistribution of Mn(II) when in

dx.doi.org/10.1021/ic200307g | Inorg. Chem. 2012, 51, 2747−2756

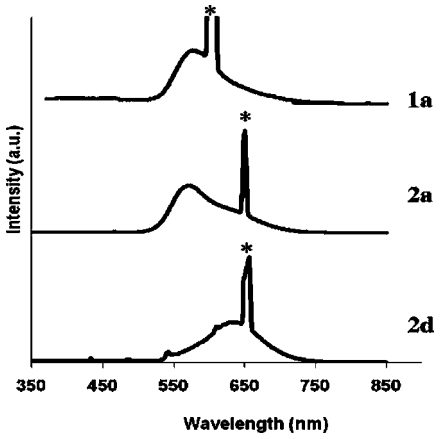

Figure 5. Room temperature solid state PL spectra of **1a**, **2a**, and **2d** as mulls in oil. The peaks labeled * arise from the different mineral oils used for sample preparation.

solution, as has been observed for Mn-Cd-E.[26] The PL data for solid samples of **2d** are also similar to those observed for solution data, with an emission observed at 640 nm. Emission at 640 nm has also been observed in related nanoparticle samples.[22] This phenomenon is usually observed with higher Mn(II) content and the close proximity of the paramagnetic centers within the nanoparticle core, resulting in direct Mn−Mn coupling[22] and related Mn-E (E = S, Se) interactions.[43]

When the amount of Mn(II) is lowest as in **1a**, a single emission is observed at 590 nm. The complete disappearance of emission at 590 nm and the emergence of a single transition at 730 nm when the amount of Mn(II) is increased in the cluster core would arise as a results of Mn−Mn coupling interactions in these clusters. A similar trend is observed for the selenium containing clusters **2a**-**d** with the only difference being the emission peak maximum at a lower wavelength. The red shift in emission displayed by the clusters **1c**-**d** (730 nm) in comparison with cluster **2c**-**d** (640 nm) is likely due to the change in the tetrahedral ligand field splitting when sulfide ligands are substituted with selenide ligands. Unlike other Mn(II) containing ZnE nanoparticles, the molecular clusters **1**-**2** also have two chloride ligands within the coordination sphere of the manganese centers which may also play a role in the observed PL data.

Metal Type Assignment by Quantum Chemical Calculations. Quantum chemical calculations at DFT level (program system TURBOMOLE,[31] BP86,[32] and B3LYP[33] functionals, def-SV(P) bases and respective Coulomb fitting bases[34]) were carried out to address the following questions: (a) Is the facile site exchange of Zn(II) with Mn(II) in $(tmeda)_6Zn_{14-x}Mn_xE_{13}Cl_2$ confirmed by quantum-chemically obtained data of exchange reactions? (b) Can we identify preferred sites for Mn(II) from calculated energies when neglecting pair interactions such as antiferromagnetic coupling? (c) Do these interactions significantly influence the preferences identified in b? We restrict considerations to E = S and briefly discuss the case E = Se in the end; for simplicity, the structures are labeled by the metal atoms only.

Facile exchange of Zn with Mn corresponds to low energies for reactions involving different compositions, for example, the reaction of the species with x Mn and $(14-x)$ Zn atoms, x = 1,2,...,7, to species with more ($m = x + 1,...,8$) or less ($l = 0,...,x-1$) Mn atoms,

$$Zn_{14-x}Mn_x \rightarrow aZn_{14-m}Mn_m + bZn_{14-l}Mn_l \qquad (2)$$

Further, in case of facile exchangeability of Zn and Mn significant changes in Zn/Mn−S and Zn/Mn−Cl distances are expected only for the positions, where the metal is exchanged (increase by a few pm when exchanging Zn with Mn, because of the larger ionic radius for the latter), but not for the unchanged positions.

For both criteria the most stable conformation for each composition has to be identified, which is not easy, as for the present systems effects of magnetic coupling cannot be neglected, in particular for those with a higher number of Mn atoms. For instance, in case of Zn_6Mn_8 the energy difference (B3-LYP, fixed structure parameters) between the high-spin case and the energetically most favorable (see below) low-spin case (broken-symmetry, i.e., antiparallel orientation of spins for different atoms[44]) amounts to about 100 kJ/mol. Moreover, only for the low-spin case one gets consistent errors in bond distances for different Mn content. In Table 5 we list the mean deviations (with respect to the experimentally determined values) of Mn−S and Zn−S distances for $Zn_{12}Mn_2$ and Zn_6Mn_8 calculated with functionals BP86 and B3LYP for the high-spin case and the most promising (see below) low-spin case. It is evident, that errors are similar for the two species only for the low-spin cases, and further, that they are smaller for BP86 than for B3LYP; this is in line with previous experiences.[45] The energy difference between spin-states in contrast is known to be overestimated with BP86, whereas the B3LYP functional was documented to give reasonable results, also for the present combination of elements (Mn/S).[45] It was thus decided to use B3LYP for energy differences, but BP86 for optimization of structure parameters.

As both distribution of Mn/Zn atoms and spin orientation of the different Mn atoms are unknown, a comparably large number of calculations would be necessary. Even if only the eight positions in question (those labeled in Figure 6) are considered, this amounts to 3^8 = 6561 calculations, as each of the eight positions may be occupied by either Zn or Mn (d^5-configuration, spin-up) or Mn (d^5-configuration, spin-down). According to the tasks formulated above, it is reasonable to

Table 5. BP86 and B3LYP Mean (Mean Absolute) Errors[a] in Metal−X (X = S, Cl) Distances of the Mn_2Zn_{12} and the Mn_8Zn_6 Species[b]

	BP86			B3LYP		
	type 1a	type 1b	type 2	type 1a	type 1b	type 2
$Zn_{12}Mn_2$, antiparallel	2.1(4.4)	0.5(2.0)	1.6(1.7)	5.7(7.1)	2.1(2.6)	2.8(2.8)
Zn_6Mn_8, parallel	6.3(7.0)		1.9(1.9)	9.8(10.3)		2.9(2.9)
Zn_6Mn_8, antiparallel	2.5(3.3)		1.9(1.9)	8.4(8.9)		2.9(2.9)

[a]In pm. [b]The Mn_8Zn_6 species being calculated with parallel and with antiparallel orientation of the spins of different Mn atoms. "Type 1a" denotes the distances from sulfur/chlorine to those of the metal positions 1−8 that are occupied by Mn, type 1b to those occupied by Zn; "type 2" covers the 12 distances from sulfur to metal positions that are occupied by Zn in both cases.

dx.doi.org/10.1021/ic200307g | Inorg. Chem. 2012, 51, 2747−2756

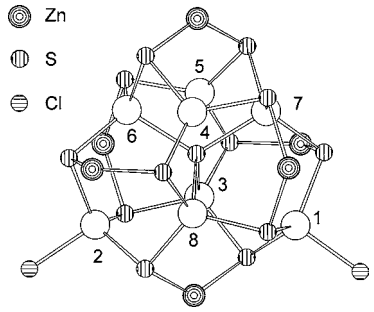

Figure 6. Core structure of $(tmeda)_6Zn_{14-x}Mn_xE_{13}Cl_2$. The eight positions labeled by numbers are occupied by either Mn or Zn.

divide the relative energies of the different distributions in a part that neglects pair-interactions, and a part describing the pair interactions; this dramatically reduces the number of calculations and further allows for estimation of the influence of pair-interactions on the metal distribution.

We start from Zn_{14} and replace only one Zn atom with Mn, in eight separate single-point calculations (using the X-ray structure parameters of $Zn_{12}Mn_2$) for the eight positions in question (Figure 6). In this way one can obtain the energetic sequence of positions without accounting for pair interactions, that is, without considering antiferromagnetic coupling of different Mn(II) centers. The relative energies, see Supporting Information, Table S2, reveal the following picture: replacement of Zn with Mn is least favorable for positions 4 and 5, where the metal atom binds to three sulfur centers (i). For positions 3 and 6 to 8 this replacement is more favorable than for positions 4 or 5 by 12−14 kJ/mol (ii); here the metal atom binds to four sulfurs. Replacement is most favorable for positions 1 and 2, at 29 and 26 kJ/mol, for which the metal atom binds to three sulfur atoms and one chlorine (iii). This follows the general trend in the coordination chemistry of these two metals and is not unexpected: the electron affinity of the environment of the metal atom increases from (i) to (ii) as the number of electronegative bond partners increases from (i) to (ii), and the electronegativity of one bond partner from (ii) to (iii). This leads to a larger energy gain for Mn than for Zn, as the electron-donating 4s orbital is less stable for Mn than for Zn. So, without regarding pair-interactions one expects positions 1 and 2 to be occupied by Mn first, 3 and 6 to 8 next, and finally 4 and 5. For instance, for Zn_8Mn_6 one would expect Mn at positions 1−3 and 6−8 from this consideration.

As interactions between neighboring Mn atoms are comparably large (see above) this picture has to be refined. For the calculation and discussion of pair interactions we introduce the following short-hand notation for the characterization of the isomers. We only denote those of the eight positions that are occupied by Mn; distinguishing between spin-down and spin-up is noted by underlining/not underlining the respective position number. As an example "1$\underline{2}$8" indicates that in the respective isomer positions one and eight are occupied by Mn (spin up), position two by Mn (spin down) and three to seven by Zn. The numbering refers to those outlined in Figure 6.

The following screening procedure was applied first, using the structure parameters of $Zn_{12}Mn_2$ from the X-ray analysis: The relative energy of each isomer was approximated by the energy change E_1 when exchanging single Zn by Mn, for example,

$$E_1(1\underline{2}8) = E_1(1) + E_1(2) + E_1(8) \quad (3)$$

plus the energy gain by the antiferromagnetic coupling, E_2, approximately accounted for in terms of atom pairs with different spin orientation,

$$E_2(1\underline{2}8) = E_2(12) + E_2(28) \quad (4)$$

E_1 (1) to E_1 (8) are the energies of the eight different isomers of Mn_1Zn_{13}· with respect to the least stable one, that is, the energies discussed in the previous section. E_2 (12) to E_2 (78) are the energy differences between the high-spin and the broken-symmetry low-spin state of the respective isomer, for example, E_2 (12) = E (12)-E (1$\underline{2}$) using the above notation; they are listed in the Supporting Information, Table S3 and amount to up to 11 kJ/mol (e.g., between positions 5 and 6). By calculation of $E = E_1 + E_2$ it is possible to estimate the energetic sequence within each given composition. This estimation reproduces the relative energies obtained by explicit calculation of the respective isomers with errors of less than about 5 kJ/mol (see Supporting Information, Figure S5). The resulting estimated energies E are listed in Supporting Information, Table S4 for all isomers that are higher in energy than the lowest for each composition by less than 10 kJ/mol. Consideration of these favorable isomers shows the following trends: If two Mn atoms are present, they probably occupy positions 1 and 2; the isomer lowest in energy that breaks this rule is 1$\underline{7}$ (+8 kJ/mol). This is in accordance to the consideration neglecting pair interactions and also to the assignment based on the crystallographic refinement of **1a** and **2a** although it is important to note that these clusters are prepared under kinetically controlled reactions conditions. The third and also the fourth Mn atom show a preference for positions 3 or 6−8. Isomers with Mn at positions 4 or 5 are higher in energy by about 10 kJ/mol at least. For more than four Mn atoms, significant preferences (apart from those for positions 1 and 2) could not be identified.

For the most stable isomer of each composition found this way, the structure parameters were optimized with the BP86 functional, followed by a single point calculation with B3LYP; the resulting structure parameters as well as BP86 and B3LYP total energies are listed in Supporting Information, Table S5. The latter were used to calculate energies for all possible reactions according to eq 2. To give an example, for Mn_2Zn_{12} we considered the 14 reactions leading to $1/3Zn_{14}$ + $2/3$ $Zn_{11}Mn_3$,..., $6/7$ $Zn_{13}Mn$ + $1/7$ Zn_6Mn_8. The relative stability of each composition is then the lowest of all reaction energies for the respective composition; if this energy is positive, the species is stable with respect to any reaction according to eq 2; smallness of this number for all compositions corresponds to nonpreference of a specific composition and thus to facile exchange of metal atoms. The lowest reaction energies for each composition are listed in Table 6. Indeed, all reaction energies are very small, absolute values are smaller than 5 kJ/mol, which is smaller than the accuracy of DFT. Thus, no preference for a specific composition could be identified; Mn and Zn apparently are easily exchangeable.

This is also reflected by the changes in structure parameters. As noted above, exchanging Zn with Mn ideally should not affect M−S distances greatly other than the positions where the metal atoms are exchanged. In Table 7 we list for the "best" isomer (see above) of each composition the average changes in M−S distances with respect to Zn_{14} ("type 1a" for the positions 1−8 occupied by Mn; "type 1b" for the positions occupied by Zn within positions 1−8; "type 2" for the other metal positions, which are always occupied by Zn). As expected, the influence of

dx.doi.org/10.1021/ic200307g | Inorg. Chem. 2012, 51, 2747−2756

Table 6. Most Favorable Isomers for Each Composition[a]

cluster	configuration	E_{reac}	products
$Zn_{13}Mn_1$	1	0.73	$^1/_2Zn_{14} + {}^1/_2Zn_{12}Mn_2$
$Zn_{12}Mn_2$	12	3.14	$^1/_2Zn_{13}Mn_1 + {}^1/_2Zn_{11}Mn_3$
$Zn_{11}Mn_3$	128	1.14	$^1/_2Zn_{12}Mn_2 + {}^1/_2Zn_{10}Mn_4$
$Zn_{10}Mn_4$	1238	1.61	$^3/_4Zn_{11}Mn_3 + {}^1/_4Zn_7Mn_7$
Zn_9Mn_5	12478	−0.42	$^1/_2Zn_8Mn_6 + {}^1/_4Zn_{10}Mn_4$
Zn_8Mn_6	124678	−1.86	$^4/_5Zn_7Mn_7 + {}^1/_5Zn_{10}Mn_2$
Zn_7Mn_7	1234678	3.45	$^1/_2Zn_8Mn_6 + {}^1/_2Zn_6Mn_8$
Zn_6Mn_8	12345678		

[a]The configurations of the respective isomers are given in column 2 (for notation see text), the lowest energies for reactions according to eq 2 (E_{reac}, in kJ/mol) in column 3 and the corresponding reaction products in column 4. A positive energy means that the reaction is endothermic, i.e., that the species is stable with respect to all reactions according to eq 2.

Table 7. BP86 Mean (Mean Average) Values[a] of Changes in Metal−X (X = S, Cl) Distances of the Mn_xZn_{14-x} with Respect to Zn_{14}[b]

	type 1a	type 1b	type 2
$Zn_{13}Mn_1$	6.1(6.1)	0.1(0.2)	−0.1(0.1)
$Zn_{12}Mn_2$	6.0(6.0)	0.2(0.4)	−0.1(0.1)
$Zn_{11}Mn_3$	5.1(5.2)	0.2(0.7)	−0.1(0.2)
$Zn_{10}Mn_4$	4.7(4.7)	0.1(0.8)	0.0(0.2)
Zn_9Mn_5	4.5(4.5)	0.6(2.5)	−0.1(0.2)
Zn_8Mn_6	4.1(4.1)	0.6(2.6)	0.0(0.3)
Zn_7Mn_7	4.0(4.0)	−0.4(0.4)	0.1(0.2)
Zn_6Mn_8	3.3(3.3)		0.1(0.2)

[a]In pm. [b]For definition of bond types (1a, 1b, 2) see Table 5.

metal exchange on unchanged positions is small (typically below 1 pm). Exchanging Zn with Mn elongates the bonds for the respective positions by 3−6 pm.

For the selenium compounds, the situation is expected to be very similar, as can be seen from the similarity of the energies for Se and S, for example, $E_1(1)$ = 23 kJ/mol (29 kJ/mol for S, see above), and $E_2(56)$ = 10 kJ/mol (11 kJ/mol for S, see above).

CONCLUSION

The chalcogenolate complexes $(tmeda)Zn(ESiMe_3)_2$ (E = S, Se) have been utilized as molecular precursors for the preparation of the ternary nanoclusters, $(tmeda)_6Zn_{14-x}Mn_xE_{13}Cl_2$ where the value of x varies from ∼2 to as high as ∼8. Using a low temperature synthetic method, we have been able to incorporate Mn(II) into well-defined ZnS and ZnSe cluster frameworks. DFT calculations allow for the following conclusions: (a) Exchange of Zn with Mn is easily feasible. (b) If one or two Mn atoms are present, they most likely will occupy positions 1 and 2, which is also supported by the crystallographic data. In case of three (four) Mn atoms one (two) additional positions from 3, 6, 7, or 8 will be occupied by Mn. In the case of more than four Mn atoms no clear preferences among positions 3−8 can be found. Positions 4 or 5, which have lower coordination numbers coordinated, may be occupied by Mn, which is a consequence of comparably strong interaction between Mn atoms of different spin orientation. The photoluminescence properties of these complexes show marked differences based on the amount of Mn(II) incorporated.

ASSOCIATED CONTENT

Supporting Information

Crystallographic information files for **1a**, **2a**, **2d**, **3**, and **4** in CIF format, ^{1}H NMR spectra of **3** and **4**, UV−visible absorption, PLE, and PL spectra for **1b**, **1c**, **2b**, **2c**, and details and parameters for the quantum chemical calculations. This material is available free of charge via the Internet at http://pubs.acs.org.

AUTHOR INFORMATION

Corresponding Author

*E-mail: florian.weigend@kit.edu (F.W.), corrigan@uwo.ca (J.F.C.).

ACKNOWLEDGMENTS

We gratefully acknowledge the Natural Sciences and Engineering Research Council of Canada (NSERC) for financial support of this research and equipment funding. NSERC, the Government of Ontario, The University of Western Ontario, and the Canada Foundation for Innovation are thanked for equipment funding. J.F.C. thanks the Karlsruhe Institute of Technology for a Guest Professorship. We thank David Dodd and Professor Robert H. E. Hudson (Western) for access and assistance with the photoluminescence measurements.

REFERENCES

(1) (a) Tran, D. T. T.; Taylor, N. J.; Corrigan, J. F. *Angew. Chem., Int. Ed.* **2000**, *39*, 935−937. (b) Tran, D. T. T.; Beltran, L. M.; Kowalchuk, C. M.; Trefiak, N. R.; Taylor, N. J.; Corrigan, J. F. *Inorg. Chem.* **2002**, *41*, 5693−5698.

(2) DeGroot, M. W.; Taylor, N. J.; Corrigan, J. F. *J. Mater. Chem.* **2004**, *14*, 654−660.

(3) DeGroot, M. W.; Taylor, N. J.; Corrigan, J. F. *Inorg. Chem.* **2005**, *44*, 5447−5458.

(4) (a) DeGroot, M. W.; Corrigan, J. F. *Angew. Chem., Int. Ed.* **2004**, *43*, 5355−5357. (b) DeGroot, M. W.; Taylor, N. J.; Corrigan, J. F. *J. Am. Chem. Soc.* **2003**, *125*, 864−865. (c) DeGroot, M. W.; Atkins, K. M.; Borecki, A.; Rösner, H.; Corrigan, J. F. *J. Mater. Chem.* **2008**, *18*, 1123−1130.

(5) (a) Komuro, T.; Matsuo, T.; Kawaguchi, H.; Tatsumi, K. *J. Chem. Soc., Dalton Trans.* **2004**, *10*, 1618−1625. (b) Komuro, T.; Matsuo, T.; Kawaguchi, H.; Tatsumi, K. *J. Chem. Commun.* **2002**, *9*, 988−989. (c) Komuro, T.; Matsuo, T.; Kawaguchi, H.; Tatsumi, K. *Angew. Chem., Int. Ed.* **2003**, *42*, 465−468.

(6) (a) Sommer, H.; Eichhöfer, A.; Drebov, N.; Ahlrichs, R.; Fenske, D. *Eur. J. Inorg. Chem.* **2008**, *32*, 5138−5145. (b) Bechlars, B.; Issac, I.; Feuerhake, R.; Clerac, R.; Fuhr, O.; Fenske, D. *Eur. J. Inorg. Chem.* **2008**, *10*, 1632−1644. (c) Feuerhake, R.; Fenske, D. *Z. Anorg. Allg. Chem.* **2003**, *629*, 2317−2324. (d) Eichhöfer, A.; Fenske, D. *J. Chem. Soc., Dalton Trans.* **2000**, 941−944.

(7) DeGroot, M. W.; Corrigan, J. F. *Z. Anorg. Allg. Chem.* **2006**, *632*, 19−29.

(8) Borecki, A.; Corrigan, J. F. *Inorg. Chem.* **2007**, *46*, 2478−2484.

(9) Furdyna, J. K., Kossut, J., Eds.; *Dilute Magnetic Semiconductors*; Academic Press: New York, 1988; Vol. 25.

(10) Alivisatos, A. P. *Science* **1996**, *271*, 933−937.

(11) Michalet, X.; Pinaud, F. F.; Bentolila, L. A.; Tsay, J. M.; Doose, S.; Li, J. J.; Sundaresan, G.; Wu, A. M.; Gambhir, S. S.; Weiss, S. *Nature* **2007**, *447*, 441−446.

(12) Gur, I.; Fromer, N. A.; Geier, M. L.; Alivisatos, A. P. *Science* **2005**, *310*, 462−465.

(13) Bhargava, R. N.; Gallagher, D.; Hong, X.; Nurmikko, A. *Phys. Rev. Lett.* **1994**, *72*, 416−419.

(14) Norris, D. J.; Yao, N.; Charnock, F. T.; Kennedy, T. A. *Nano Lett.* **2001**, *1*, 3−7.

(15) Stowell, C. A.; Wiacek, R. J.; Sauders, A. E.; Korgel, B. A. *Nano Lett.* **2003**, *3*, 1441−1447.
(16) Santra, S.; Yang, H.; Holloway, P. H.; Stanley, J. T.; Mericle, R. A. *J. Am. Chem. Soc.* **2005**, *127*, 1656−1657.
(17) Norberg, N. S.; Parks, G. L.; Salley, G. M.; Gamelin, D. R. *J. Am. Chem. Soc.* **2006**, *128*, 13195−13203.
(18) Sapra, S.; Prakash, A.; Ghangrekar, A.; Periasamy, N.; Sarma, D. D. *J. Phys. Chem. B* **2005**, *109*, 1663−1668.
(19) Pradhan, N.; Goorskey, D.; Thessing, J.; Peng, X. *J. Am. Chem. Soc.* **2005**, *127*, 17586−17587.
(20) Erwin, S. C.; Zu, L.; Haftel, M. I.; Efros, A. L.; Kennedy, T. A.; Norris, D. J. *Nature* **2005**, *436*, 91−94.
(21) Yang, Y.; Chen, O.; Angerhofer, A.; Cao, C. J. *J. Am. Chem. Soc.* **2006**, *128*, 12428−12429.
(22) Pradhan, N.; Peng, X. *J. Am. Chem. Soc.* **2007**, *129*, 3339−3347.
(23) Nag, A.; Sapra, S.; Nagamani, C.; Sharma, A.; Pradhan, N.; Bhat, S. V.; Sarma, D. D. *Chem. Mater.* **2007**, *19*, 3252−3259.
(24) Norris, D. J.; Efros, Al. L.; Erwin, S. C. *Science* **2008**, *319*, 1776−1779.
(25) Beaulac, R.; Archer, P. I.; Ochsenbein, S. T.; Gamelin, D. R. *Adv. Funct. Mater.* **2008**, *18*, 3873−3891.
(26) Eichhöfer, A.; Hampe, O.; Lebedkin, S.; Weigend, F. *Inorg. Chem.* **2010**, *49*, 7331−7339.
(27) Pangborn, A. B.; Giardello, M. A.; Grubbs, R. H.; Rosen, R. K.; Timmers, F. J. *Organometallics* **1996**, *15*, 1518−1520.
(28) So, J.; Boudjouk, P. *Synthesis* **1989**, 306−307.
(29) DeGroot, M. W.; Corrigan, J. F. *Organometallics* **2005**, *24*, 3378−3385.
(30) (a) Sheldrick, G. M. *SHELXTL PC, An Integrated System for Solving, Refining, and Displaying Crystal Structures from Diffraction Data*, version 6.1; Bruker Analytical X-ray Systems: Madison, WI, 2000; (b) Sheldrick, G. M. *Acta Crystallogr., Sect. A* **2008**, *64*, 112−122.
(31) *TURBOMOLE*, V6.1; Turbomole GmbH: Karlsruhe, Germany, 2010; http://www.turbomole.de. TURBOMOLE is a development of the University of Karlsruhe and the Forschungszentrum Karlsruhe 1989−2007, Turbomole GmbH since 2007.
(32) (a) Becke, A. D. *Phys. Rev. A* **1988**, *38*, 3098−3100. (b) Perdew, J. P. *Phys. Rev. B* **1996**, *33*, 8822−8824.
(33) Lee, C.; Yang, W.; Parr, R. G. *Phys. Rev. B 37* **1988**, 785−789.
(34) (a) Weigend, F.; Ahlrichs, R. *Phys. Chem. Chem. Phys.* **2005**, *7*, 3297−3305. (b) Weigend, F. *Phys. Chem. Chem. Phys.* **2006**, *8*, 1057.
(35) Pfistner, H.; Fenske, D. *Z. Anorg. Allg. Chem.* **2001**, *627*, 575−582.
(36) *CRC Handbook of Chemistry & Physics*, 88th ed.; Lide, D. R., Ed.; CRC Press: Boca Raton, FL, 2006.
(37) Stephan, H. O.; Henkel, G. *Polyhedron* **1996**, *15*, 501−511.
(38) Eichhöfer, A.; Wood, P. T.; Viswanath, R. N.; Mole, R. A. *Chem. Commun.* **2008**, *13*, 1596−1598.
(39) Ali, B.; Dance, I. G.; Craig, D. C.; Scudder, M. L. *J. Chem. Soc., Dalton. Trans.* **1998**, 1661−1667.
(40) Nyman, M. D.; Hampden-Smith, M. J.; Duesler, E. N. *Inorg. Chem.* **1996**, *35*, 802−803.
(41) Eichhöfer, A.; Fenske, D.; Pfistner, H.; Wunder, M. *Z. Anorg. Allg. Chem.* **1998**, *624*, 1909−1914.
(42) Graf, C.; Hofmann, A.; Ackermann, T.; Boeglin, C.; Viswanatha, R.; Peng, X.; Rodrigues, A. F.; Nolting, F.; Rühl, E. *Adv. Funct. Mater.* **2009**, *19*, 2501−2510.
(43) Karar, N.; Singh, F.; Mehta, B. R. *J. Appl. Phys.* **2004**, *95*, 656−660.
(44) Ruiz, E.; Cano, J.; Alvarez, S.; Alemany, P. *J. Comput. Chem.* **1999**, *20*, 1301−1400.
(45) von Hänisch, C.; Weigend, F.; Clérac, R. *Inorg. Chem.* **2008**, *47*, 1460−1464.